NASA TECHNICAL MEMORANDUM

NASA TM X-73471

NASA TM X-73471

ION TEMPERATURES IN HIP-1 AND SUMMA FROM CHARGE-EXCHANGE NEUTRAL OPTICAL EMISSION SPECTRA

by R. W. Patch and M. R. Lauver
Lewis Research Center
Cleveland, C 44135

TECHNICAL PAPER presented at
Conference on Diagnostics of High Temperature Plasmas
sponsored by the Division of Plasma Physics
of the American Physical Society
Knoxville, Tennessee, January 7-9, 1976

ION TEMPERATURES IN HIP-1 AND SUMMA FROM CHARGE-EXCHANGE NEUTRAL OPTICAL EMISSION SPECTRA

by R. W. Patch and M. R. Lauver

Lewis Research Center

SUMMARY

Ion temperatures were obtained from observations of the H_α, D_α, and He 587.6 nm lines emitted from hydrogen, deuterium, and helium plasmas in the SUMMA and HIP-1 mirror devices at Lewis Research Center. Steady-state $\vec{\epsilon} \times \vec{B}$ discharges were formed by applying a radially inward dc electric field between cylindrical or annular anodes and hollow cathodes located at the peaks of the mirrors. The ion temperatures were found from the Doppler broadening of the charge-exchange components of spectral lines.

A statistical method was developed for obtaining scaling relations of ion temperature as a function of current, voltage, and magnetic flux density. The method was applied to hydrogen with ion temperatures between 169 and 854 eV, deuterium with temperatures between 268 and 650 eV, and helium with temperatures between 597 and 4927 eV.

Derivations are given that take into account for the first time triangular monochromator slit functions, loss cones, and superimposed charge-exchange processes. In addition, the Doppler broadening was found to be sensitive to the influence of drift on charge-exchange cross section. The effects of finite ion-cyclotron radius, cascading, and delayed emission are reviewed. Including the effect of slit function and loss cones reduced the ion temperature. In the zero-ion-cyclotron-radius approximation including drift increased the ion temperature. In the finite-ion-cyclotron-radius approximation an additional physical phenomenon tended to decrease the ion temperature at high ion temperatures.

E-8604

INTRODUCTION

This report presents results of research undertaken to measure and obtain scaling relations for ion temperatures in the Hot Ion Plasma 1 (HIP-1) apparatus and the Superconducting Magnetic Mirror Apparatus (SUMMA) at NASA Lewis Research Center. Both HIP-1 and SUMMA are magnetic mirror facilities. HIP-1 has copper magnet windings whereas SUMMA has superconducting magnet windings. In both facilities a steady state discharge is formed by applying a radially inward dc electric field between cylindrical anodes and hollow cathodes located at the peaks of the mirror. The perpendicular electric and magnetic fields cause the electrons and

ions of the plasma to drift azimuthally with approximately the same velocity, corresponding to an ion drift energy of as much as several kilovolts. In addition, it appears that turbulence occurs, which results in ion heating (ref. 1). The ion temperatures in such devices are many times the electron temperatures.

The approach used in measuring ion temperatures was to observe emission from the Doppler-broadened charge-exchange neutral spectra of atomic lines. The method used in this report for obtaining ion temperatures from the measured width (or second moment) of such lines was given in reference 2 but was extended to deuterium for the present work.

Statistical methods were used to obtain improved scaling relations for ion temperature from H_α and He 587.6 nm SUMMA data (ref. 2) and for similar data from H_α and D_α HIP-1 observations. The SUMMA data were obtained for uncooled tungsten hollow cylindrical cathodes and cooled anodes, and the HIP-1 data were obtained for tungsten-coated water-cooled copper cathodes and ring anodes.

The scope of the scaling relation study is limited to average ion temperature in pure H_2, D_2, and He plasmas at the magnetic midplane. The averages are obtained by observing the emission spectra across a diameter and are inherently heavily weighted in favor of the center of the plasma, where most of the light intensity originates. No attempts were made to invert the observed spectral intensities to get intensity and hence ion temperature as a function of radius because an Abel inversion is not applicable due to the anisotropy of the spectral emission.

Also contained in this report are some advances in the theory of broadening of charge-exchange neutral spectra from rotating plasmas in mirror machines. In the future these advances will be used to obtain more accurate ion temperatures than can be obtained by the method in reference 2.

Closely related experimental efforts on charge-exchange neutral Doppler broadening were presented in references 3 to 5. An influence of finite lifetime of excited states was observed in the experiment of reference 6. A plasma model which includes configuration as well as velocity space (ref. 7) has been recently adapted to Doppler broadening. The influence of lifetime of excited states, finite cyclotron radius, and azimuthal drift was studied in reference 8.

The influence of drift on the σv correction to line shape is presented herein as an extension to reference 2. The influence on broadening of cut-off of velocity distribution due to loss cones is also discussed.

The authors are indebted to Dr. Norman Tolk of Bell Telephone Laboratories for measuring the ratio of excitation cross sections of the He 587.6 and He 667.8 nanometer lines.

EXPERIMENTAL APPARATUS

SUMMA

Magnets. - The Superconducting Magnetic Mirror Apparatus (SUMMA) (ref. 10) includes four superconducting solenoidal magnets of which the inboard two were used for present study (see fig. 1). Each magnet has an inner, a middle, and an outer winding, which were independently powered. The two inboard magnets alone produce maximum steady flux densities of about 5.2 T and 3.5 T at the mirrors and midplane, respectively. The average mirror ratio R was 1.55 (symbols are given in appendix A).

Plasma test section. - A schematic view of the plasma test section is shown in figure 1. The discharge chamber is a cylinder 3.75 m in length and 36.6 cm in diameter made from type 304 stainless steel. Two 25.4 cm diffusion pumps provided a base pressure of 5×10^{-7} torr.

Electrode assembly. - The electrode arrangement is also shown schematically in figure 1. More detail is shown in figure 2. Gas is introduced through the uncooled tungsten cathodes (1.27 cm o.d.) to produce a hollow-cathode discharge. The water-cooled copper anode rings have 2.9 cm and 5.1 cm inside and outside diameters, resepectively. They are electrically grounded to the test section walls. The electrically floating shield protects a cathode holder from heavy particle bombardment and helps inhibit arcing from the cathode to the electrically grounded back flange. The shield was constructed of tungsten-coated copper and cooled by water. The cathodes are connected in parallel to a single dc power supply.

HIP-1

Magnets. - In this apparatus two water-cooled copper solenoidal magnets are used to produce a maximum steady flux density of 1.18 T at the midplane and 2.15 T at the mirrors for a fixed mirror ratio R of 1.82.

Plasma test section. - The discharge chamber is a cylinder 1.63 m in length and 25 cm in diameter made from type 304 stainless steel. Two 35.6-cm and two 15.2-cm diffusion pumps provide a base pressure of 5×10^{-7} torr.

Electrode assembly. - The two electrode assemblies, of which one is shown in figure 3, are placed near the mirrors in an arrangement similar to SUMMA. The gas supply to the hollow cathodes is similar to SUMMA, but the materials, cooling and dimensions of the electrodes differ. The cathodes (W.C. no. 3 in ref. 9) have inside and outside diameters of 2.54 cm and 4.45 cm, respectively. The anodes have inside and outside diameters of 6.35 cm and 8.25 cm, respectively. The cathodes, anodes, and floating shields are all water-cooled copper with plasma flame-sprayed coatings of tungsten (see fig. 3). Electrical connections are similar to SUMMA.

Diagnostic Equipment

The same apparatus for emission spectroscopy was used in SUMMA and HIP-1 and is shown in figure 4. It was located at the test-section midplane and viewed the plasma perpendicular to the magnet axis. The vertical centerplane (a vertical plane containing the magnetic axis) was focussed on the entrance slit of the monochromator with a lens. Between the lens and the entrance slit the beam was rotated 90° with a beam rotator. A stop was provided to reduce the vertical height of the beam. The beam cross-section at the vertical centerplane was determined by the size and shape of the entrance slit. The beam cross-section was approximately 2 mm in the vertical direction and 2.6 cm parallel to the magnetic axis. An adjustable screw at the base of the monochromator table was used to make vertical scans. For the work reported here the monochromator was focused across the centerline of the plasma so the quantity y in figure 4 was zero. The grating monochromator employed an f/8.6 1/2 meter Ebert mounting with curved slits. The reciprocal linear dispersion was 1.6 nm/mm in first order. A photomultiplier with extended S-20 photocathode was magnetically shielded and cooled with air that came from a vortex tube refrigerator.

In SUMMA a floating electrical probe equipped for rapid traverse of the plasma was installed for several runs.

TEMPERATURE SCALING RELATIONS

Theory

Scaling relations of the form

$$T_i = 10^{b_0} I^{b_1} V^{b_2} B^{b_3} \qquad (1)$$

were found in HIP-1 (ref. 9), where T_i is ion temperature at the magnetic midplane, I is total current into the cathodes, V is electrode voltage, B is midplane magnetic flux density, and b_0 through b_3 are constants. The form of equation (1) was found by the process of holding two independent variables fixed and varying the third. If equation (1) is inexact, such a procedure may bias the data. Use of a regression analysis makes the procedure of reference 9 unnecessary and makes it possible to take the data without biasing it and without the experimental complication of holding two independent variables fixed.

To do a regression analysis, we write equation (1) in logarithm form:

$$\log T_i = b_0 + b_1 \log I + b_2 \log V + b_3 \log B \qquad (2)$$

This is the standard form of the regression equation for triple linear

correlation (ref. 11), where log I, log V, and log B are independent variables, b_1 through b_3 are coefficients of net regression, and log T_i is the dependent variable. The coefficients of net regression may be found by the methods in reference 11.

The use of the above method makes it possible to obtain scaling relations from old data where the independent variables were not held fixed.

To estimate the reliability of the regression coefficients and the resulting values of T_i, a statistical analysis (refs. 11, 12, 13) is useful. The multiple regression and statistical analyses were performed with three programs for a high-speed digital computer. Only one of these has been documented (ref. 12).

Results and Discussion

Hydrogen and helium were run in SUMMA. In HIP-1 these two gases and deuterium were run. Test conditions are given in table I. The data for HIP-1 are for only one anode ring installed. Observations were made of the H_α, D_α, and He 587.6 nm lines. A typical observation of H_α is shown in figure 5 from SUMMA. No forbidden satellites due to plasma turbulence were identified.

The runs differed in the following particulars from the HIP-1 runs reported in reference 9: 1) In this report gas flow for both apparatuses was through both cathodes whereas in reference 9 it was through one cathode only, 2) In this report in order for the statistics to be meaningful each data point represents one set of experimental readings whereas in reference 9 each data point represented an average of several sets of experimental readings, 3) In this report no attempt was made to take data at any particular point if the anode current varied cyclically, whereas in reference 9 all data used in determining scaling relations was taken at the lowest anode current in the cycle, 4) In this report no attempt was made to hold two variables constant and vary a third, but this procedure was followed in reference 9.

In converting Doppler broadening to ion temperature, the methods of reference 2 were used because numerical methods for handling large amounts of data have not been developed as yet for the case involving drift and loss cones. It was assumed that the only significant reactions were

$$H_f^+ + H_2 \rightarrow H_f^* + H_2^+ \qquad \text{(I)}$$

$$D_f^+ + D_2 \rightarrow D_f^* + D_2^+ \qquad \text{(II)}$$

$$He_f^+ + He \rightarrow He_f^* + He^+ \qquad \text{(III)}$$

where subscript f stands for fast and superscript * stands for electronically excited. The only corrections made to the second moments of the charge-exchange components of the spectral lines were for fine structure, magnetic splitting, and slit function (ref. 2) and the total corrections never exceeded 11 percent. Ion temperatures were then found from figure 6, which is the same as table I of reference 2 except that D_α and D_β have been added.

The scaling relations for H^+ and He^+ in SUMMA are given in figures 7 and 8. The scaling relation for H^+ in HIP-1 is given in figure 9. For D^+ in HIP-1 the voltage was held constant, so only a double correlation was possible. It is given in figure 10. For He^+ in HIP-1 there was too small a sample to obtain a reliable scaling relation of any kind. The scatter in figures 9 and 10 is greater than in reference 9 because of differences 2) and 3) mentioned above.

A statistical summary of the T_i scaling relations is given in Table II. For H^+ in SUMMA and HIP-1 the correlations with I, V, and B were all highly significant (definitions of "significant" and "highly significant" are given in ref. 13). For He^+ in SUMMA the correlation with V was highly significant, but the correlations with I and B were not significant. This probably means that a larger sample is required, or I and B must be varied over wider ranges, or experimental variables must be measured more accurately. For HIP-1 with D^+ the correlation with I was highly significant whereas the correlation with B was only significant.

Standard deviations of coefficients of net regression are also given in Table II. With these the scaling relations may be written:

$$T_i \sim I^{0.52\pm0.10}V^{1.64\pm0.05}B^{-1.30\pm0.22} \quad (\text{SUMMA } H^+) \qquad (3)$$

$$T_i \sim I^{-0.11\pm0.24}V^{1.36\pm0.05}B^{-0.29\pm0.22} \quad (\text{SUMMA } He^+) \qquad (4)$$

$$T_i \sim I^{0.33\pm0.04}V^{1.50\pm0.10}B^{-0.49\pm0.10} \quad (\text{HIP-1 } H^+) \qquad (5)$$

$$T_i \sim I^{0.32\pm0.05}B^{-0.30\pm0.12} \quad (\text{HIP-1 } D^+) \qquad (6)$$

Equation (5) does not agree exactly with reference 9, where for slightly different conditions it was found

$$T_i \sim I^{0.3}V^{1.4}B^{-0.8} \quad (\text{HIP-1 } H^+) \qquad (7)$$

The difference in I and V exponents is within the experimental error. The cause of the discrepancy in B exponents has not been investigated.

The last column of Table II contains the standard error of estimate S_z of $\log_{10} T_i$. The relative standard error of estimate can be found from the last column and the relation

$$\frac{S_{T_i}}{T_i} = S_z \ln 10 = 2.30\, S_z \tag{8}$$

which gives

$$\frac{S_{T_i}}{T_i} = 0.0685 \quad (\text{SUMMA } H^+) \tag{9}$$

$$\frac{S_{T_i}}{T_i} = 0.104 \quad (\text{SUMMA } He^+) \tag{10}$$

$$\frac{S_{T_i}}{T_i} = 0.112 \quad (\text{HIP-1 } H^+) \tag{11}$$

$$\frac{S_{T_i}}{T_i} = 0.136 \quad (\text{HIP-1 } D^+) \tag{12}$$

Hence for H^+ in SUMMA the ion temperatures deviated on the average about 6.85% from the value estimated from the scaling relation (together with b_0).

In order to compare H^+ data from HIP-1 and SUMMA, the SUMMA data were replotted in figure 9 even though the correlating parameter is not optimum for the SUMMA data. It can be seen that the uncooled tungsten cathodes in SUMMA gave higher temperatures than the cooled tungsten-coated copper cathodes in HIP-1. This is partly due to the difference in cathode diameters as was verified by running cathodes of smaller diameter in HIP-1 (ref. 9). It may also be partly due to a higher neutral density in HIP-1 causing higher charge-exchange power loss (see ref. 9). However, HIP-1 plasmas had larger diameters than in SUMMA, which is desirable.

The results in figures 7, 9, and 10 should be viewed with some caution, as order-of-magnitude nonequilibrium composition calculations indicated that there could be 15 percent as much H_2^+ as H^+, so the reactions

$$H_{2f}^{+} + H_2 \rightarrow H^{*} + \text{products} \qquad \text{(IV)}$$

and similar reactions for D_{2f}^{+} may be significant although they were neglected. However, because the shape of the cross section curve for reaction IV resembles the shape for reaction I, the resulting error in T_i should not be serious.

The line shape of H_α from SUMMA agrees well with the line shape calculated from equation (B7) of reference 2 as shown in figure 11. For these conditions the fine-structure, magnetic-splitting, and slit-function corrections were negligible. The effect of azimuthal drift was neglected in computing the curve labeled "calculated" in figure 11.

IMPROVED THEORY OF LINE SHAPES AND SECOND MOMENTS

A theory of line shapes and second moments of charge-exchange neutral spectra was given in reference 2. In this section the treatment of reference 2 is reviewed, and the slit function and splitting corrections are put on a sounder mathematical basis without changing the results. Additional effects and assumptions are considered.

Line Shapes

In most charge-exchange collisions involving electron exchange, the velocity of the projectile is little affected by the collision (ref. 14). Consequently, for a charge-exchange process of the type

$$A_f^{+} + B \rightarrow A_f^{*} + B^{+} \qquad \text{(V)}$$

where the projectile A^+ is a positive atomic ion, the target B is a neutral atom or molecule, A^* is an electronically excited charge-exchange neutral atom with the same nucleus as A^+, and B^+ is B with one electron removed, a measurement of the A^+ temperature can be obtained by measuring the line width (or second moment) of an A^* line provided the A^+ temperature is much greater than the temperature of B. The second moment of A^* is obtained theoretically by studying the Doppler-broadening of the charge-exchange component of one of its spectral lines. The Doppler-broadening appears in the line shape function.

The line shape function F is proportional to the emission intensity at a specific wavelength for an optically thin line. A typical line shape for the charge-exchange component of H_α is the wide bell-shaped curve including the two faired segments in figure 5. For analytic purposes it is convenient to normalize the line shape so that

$$\int_{-\infty}^{\infty} F(\Lambda)\, d\Lambda = 1 \tag{13}$$

where Λ is the displacement from the line center in terms of wavelength.

Convolution of Line Shapes and Slit Function

The apparent line shape F_e observed at the exit slit of a monochromator as the wavelength setting of the monochromator is changed is actually the convolution of three shapes: (1) the line shape F_3 of a fine structure component (they will be assumed to all have the same shape); (2) the line shape F_1 of the fine structure at zero temperature (actually a series of sharp peaks); and (3) the slit function S of the monochromator. The line shape F_3 is what is needed to determine the temperature.

The line shape F_1 is given by

$$F_1(\Lambda) = \sum_{i=1}^{k} I_i \delta(\Lambda - \Lambda_{oi}) \tag{14}$$

where I_i is the integrated intensity (the spectral intensity integrated over all wavelengths) of each component, δ is the Dirac delta function, Λ_{oi} is the displacement of the center of the i^{th} component from the center of the line, and the sum is over the k components. Equation (14) includes both the usual fine structure and magnetic splitting. The shape F_1 satisfies equation (13) if the I_i's are normalized by

$$\sum_{i=1}^{k} I_i = 1 \tag{15}$$

The monochromator slit function S accounts for line broadening that is due to the finite width of the entrance and exit slits, optical aberrations, and unwanted diffraction. The slit function is proportional to the response of the monochromator when set at one wavelength but illuminated by a different wavelength. Two typical slit functions are shown in figure 12. The slit function is normalized by

$$\int_{-\infty}^{\infty} S(x)\, dx = 1 \tag{16}$$

The true line shape F_r is the convolution of F_1 and F_3 (ref. 15).

$$F_r(\Lambda) = \int_{-\infty}^{\infty} F_3(\Lambda - \Lambda')F_1(\Lambda')\, d\Lambda' \tag{17}$$

The apparent line shape is the convolution of F_r and S (ref. 16).

$$F_e(\Lambda) = \int_{-\infty}^{\infty} S(\Lambda - \Lambda'')F_r(\Lambda'')\, d\Lambda'' \tag{18}$$

Substituting equation (17) into equation (18) and reversing the order of integration gives

$$F_e(\Lambda) = \int_{-\infty}^{\infty} F_1(\Lambda') \int_{-\infty}^{\infty} S(\Lambda - \Lambda'')F_3(\Lambda'' - \Lambda')\, d\Lambda''\, d\Lambda' \tag{19}$$

Making the substitutions $\Lambda' \equiv \Lambda - \Lambda'''$ and $\Lambda - \Lambda'' \equiv \Lambda''''$

$$F_e(\Lambda) = \int_{-\infty}^{\infty} F_1(\Lambda - \Lambda''') \int_{-\infty}^{\infty} S(\Lambda'''')F_3(\Lambda''' - \Lambda'''')\, d\Lambda''''\, d\Lambda''' \tag{20}$$

But the inner integral is simply the convolution of S and F_3, while the outer integral is the convolution of the inner integral and F_1. Hence $F_e(\Lambda)$ is independent of the order of convolution. This justifies the order in which the second moment corrections are made in reference 2 and in appendix C of this report.

Second Moment in the Limit of Zero Ion-Cyclotron Radius

In the determination of ion temperature from F_e, it is desirable to correct for monochromator slit function, fine structure and magnetic splitting, and the superposition of charge-exchange spectra from several reactions. These corrections are greatly facilitated if the Doppler broadening is measured in terms of the second moment instead of the half width of F. The second moment is defined by

$$\langle \Lambda^2 \rangle = \int_{-\infty}^{\infty} \Lambda^2 F\, d\Lambda \tag{21}$$

which is the average value of the square of the wavelength deviation of the line shape from its center.

No loss cones or drift. - It is shown in reference 2 that in the limit of zero ion-cyclotron radius and assuming spatial homogeneity and no loss cone or azimuthal drift that the second moment is

$$\left\langle \Lambda^2 \right\rangle_3 = \frac{2\lambda_0^2}{3Mc^2} \frac{\int_0^\infty \sigma_*(E) e^{-E/kT_i} E^2 \, dE}{\int_0^\infty \sigma_*(E) e^{-E/kT_i} E \, dE} \tag{22}$$

where the symbols are defined in appendix A, and $\left\langle \Lambda^2 \right\rangle_3$ is the second moment of F_3. Cross sections for H_α and H_β are shown in figure 13. Results from equation (22) are tabulated in reference 2 for H_α, H_β, He 587.6, and He 667.8 lines and are plotted in figure 6 of this report for H_α, H_β, D_α, D_β, He 587.6, and He 667.8 lines. In the case of the Balmer lines, the target was assumed to be H_2 or D_2.

Loss cones but no drift. - If there is no azimuthal drift but ions are lost through loss cones in velocity space, the second moment can be derived from the relation

$$\left\langle \Lambda^2 \right\rangle_3 = \frac{\lambda_0^2}{c^2} \left\langle v_x^2 \right\rangle \tag{23}$$

by assuming a Maxwell-Boltzmann velocity distribution outside the loss cones. The result is

$$\left\langle \Lambda^2 \right\rangle_3 = \left(1 + \frac{1}{2R}\right) \frac{2\lambda_0^2}{3Mc^2} \frac{\int_0^\infty \sigma_*(E) e^{-E/kT_i} E^2 \, dE}{\int_0^\infty \sigma_*(E) e^{-E/kT_i} E \, dE} \tag{24}$$

where R is the mirror ratio. This is simply (1 + 1/2R) times equation (22). Because $R > 1$, this means that $\left\langle \Lambda^2 \right\rangle_3$ will be increased. Hence, if T_i is determined from $\left\langle \Lambda^2 \right\rangle_3$, T_i will be smaller if equation (24) is used instead of equation (22).

Drift but no loss cones. - It is assumed that the plasma is spatially homogeneous, that there is a Maxwell-Boltzmann distribution of ion velocities about a uniform azimuthal drift, and that the neutrals remain stationary. If the plasma is viewed across a diameter, and the ion cyclotron radius is zero, the azimuthal drift can be replaced by a drift in the v_y direction (fig. 14), where the line of sight and magnetic axis are in the v_x and v_z directions, respectively. The case of drift but no loss cones can be derived by the same general method as in appendix B with the result

$$\left\langle \Lambda^2 \right\rangle_3 = \frac{2\lambda_0^2}{Mc^2H^2} \frac{\int_0^\infty \sigma_*(E) e^{-E/kT_i} E \left(\cosh Q - \frac{\sinh Q}{Q} \right) dE}{\int_0^\infty \sigma_*(E) e^{-E/kT_i} E \frac{\sinh Q}{Q} dE} \tag{25}$$

Hence, in general, drift affects the second moment through its influence on E, σ_*, and Q. The exception to this is the special case where $\sigma_* \sim v^{-1}$ so that the charge-exchange neutrals have a Maxwell-Boltzmann velocity distribution like the ions. In this case if observations are made perpendicular to the drift velocity (as was assumed in deriving eq. (25)), the second moment is independent of drift in the zero-ion-cyclotron radius approximation used here. However, in practical cases σ_* does not vary as v^{-1}. In fact, for H_α σ_* increases with increasing v (see fig. 13). The second moment for H_α is shown in figure 15 for no loss cones and various drift velocities. For this cross section (fig. 13) drift tends to reduce the second moment. If the drift becomes much larger than the ion thermal velocities, the v in $\sigma_*(v)v$ is almost independent of the component of v along the line of sight, so $\sigma_*(v)v$ may be regarded as a constant. Hence the second moment approaches the value for a Maxwell-Boltzmann distribution at the ion temperature.

Loss cones and drift. - If there is azimuthal drift, the loss cones are reduced in size and are no longer conical. The same basic assumptions as in the preceding section are made. This case is treated in appendix B. Based on floating probe and magnetic flux density measurements in SUMMA, a typical drift velocity is 400 000 m/sec. For this drift velocity, the effect of mirror ratio on $\left\langle \Lambda^2 \right\rangle_3$ is shown in figure 16. Here the value 1.68 of the mirror ratio is the average of the mirror ratios of HIP-1 and SUMMA. Just as for the zero drift case, the second moment is increased by the presence of loss cones. The second moment for H_α is shown in figure 17 for a mirror ratio of

1.68 and various drift velocities. The drift tends to reduce the second moment even more than in figure 15. If the drift is large enough, it makes the loss cones negligible, and the second moment approaches the Maxwell-Boltzmann limit just as in the previous case.

Corrections to Second Moment for Slit Function

A correction ε to the second moment due to monochromator slit function is derived in appendix D of reference 2 for a Gaussian slit function (see fig. 12) and is

$$\varepsilon = -\frac{W^2}{8 \ln 2} = -0.1803\ W^2 \tag{26}$$

where W is the full half width of the slit function. For many monochromators this is a good approximation for narrow entrance and exit slits of the same width.

To obtain a good signal-to-noise ratio, it is frequently necessary to use wide slits. For the ideal case of wide slits of equal width, a triangular slit function is produced (see fig. 12). In appendix C it is shown that the second moment correction for a triangular slit function is

$$\varepsilon = -\frac{W^2}{6} = -0.1667\ W^2 \tag{27}$$

Assuming the slit function correction is considerably smaller than the second moment, an average of equations (26) and (27) namely $-0.1735\ W^2$, should be accurate enough for Gaussian or triangular slit functions or slit functions intermediate between the two.

Second Moment for the General Case

In reaction (V) the target B in the case of hydrogen could be either H or H_2. The projectile A^+ could be either H^+ or H_2^+. In addition to reaction (V), two-step processes (ref. 2) may be important if the plasma is large enough or dense enough. In general, the second moments for different processes will be different. It is shown in appendix D that for n charge-exchange processes with superimposed charge-exchange spectra the second moment $\langle \Lambda^2 \rangle_{3t}$ of the total line shape is

$$\langle \Lambda^2 \rangle_{3,t} = \sum_{j=1}^{n} I_j \left(\langle \Lambda^2 \rangle_{3,j} + \Lambda_{oj}^2 \right) \tag{28}$$

where I_j is the integrated intensity for process j. Consequently, if corrections are made for splitting (appendix C of ref. 2) and monochromator slit function

$$\sum_{j=1}^{n} I_j \left(\langle \Lambda^2 \rangle_{3,j} + \Lambda_{oj}^2 \right) = \langle \Lambda^2 \rangle_1 - \sum_{i=1}^{k} I_i \Lambda_{oi} - 0.1735\ W^2 \tag{29}$$

where $\langle \Lambda^2 \rangle_1$ is the second moment observed at the exit slit of the monochromator as wavelength is scanned. Equation (29) can be solved for T_i if a table of the left hand side versus T_i is calculated and interpolated.

Effect of Finite Ion-Cyclotron Radius on Half Width

In the above derivations it was assumed that the ion-cyclotron radius was zero, although equation (29) is applicable even for finite ion cyclotron radius. Recently the problem of finite ion cyclotron radius has been treated (ref. 8) using the guiding-center model. It was assumed that (1) there was no loss cone, (2) the ions had a diffusion density profile in the radial direction, (3) the neutral concentration was constant, (4) the drift velocity of ions was $\vec{\epsilon} \times \vec{B}/B^2$, (5) the ion temperature was a constant, and (6) the charge-exchange spectra were due to

$$H_f^+ + H_2 \rightarrow H_f^* + H_2^+ \tag{VI}$$

The combination of finite ion-cyclotron radius with azimuthal drift was found to increase the half width and hence the second moment (the second moment is roughly proportional to the square of the half width). This is just the opposite of the effect of drift in the case of zero ion cyclotron radius (figs. 15 and 17). The finite radius effect can be understood from figure 18, which assumes no delay in emission by the charge-exchange neutral. The ion in the line of sight has the usual cyclotron velocity v_c. However, its guiding center is located above it and to the right and has a drift velocity v_d. When v_d is added to v_c, the resultant velocity v_r of the ion has a larger component along the line of sight than does v_c alone. Hence the spectral line is broadened. The broadening effect of drift due to finite cyclotron radius

was found dominant over the σv effect for the relatively moderate ranges of drift to random energy reported in reference 8.

Effect of Cascade on Half Width

In reference 8 the effect of delayed cascading from higher levels and of delayed emission of H_f^* were also investigated. These had little effect on the half width of the emission observed across a diameter, but caused large increases in half width for lines of sight that did not pass through the center of the plasma. Unfortunately, insufficient cross sections are available for hydrogen to evaluate cascade and delayed emission properly.

Inversion

It would be desirable to observe emission for a number of values of y (fig. 4) and then invert the spectra to obtain T_i as a function of radius. Unfortunately, an Abel inversion is not applicable to the spectral intensity because the spectral intensity is anisotropic. However, the integrated intensity (area under the spectral line profile) is isotropic so an Abel inversion is applicable to it. Nevertheless, there are obstacles to obtaining T_i as a function of radius: (1) cascading and delayed emission in hydrogen must be better evaluated, (2) it is not known with certainty what formula is a satisfactory approximation to the ion azimuthal drift velocity, and (3) numerical methods must be developed for the inversion itself. It appears that the second moment is better suited to this problem than the half width.

CONCLUDING REMARKS

The first purpose of the study was to obtain scaling relations for ion temperature by a statistical method. The ion temperatures were measured in nonequilibrium hot-ion plasmas by observing the second moments of the charge-exchange neutral components of atomic lines. These moments were then corrected for three effects and compared with moments calculated for various ion temperatures. In SUMMA, midplane ion temperatures ranged from 169 to 854 eV in hydrogen and from 666 to 4927 eV in helium. In HIP-1, midplane ion temperatures were from 170 to 607 eV in hydrogen, from 268 to 650 eV in deuterium, and from 597 to 980 eV in helium. The scaling relations were

$$T_i \sim I^{0.52\pm0.10} V^{1.64\pm0.05} B^{-1.30\pm0.22} \quad (\text{SUMMA } H^+)$$

$$T_i \sim I^{-0.11\pm0.24}{}_V 1.36\pm0.05_B{}^{-0.29\pm0.22} \quad \text{(SUMMA } He^+\text{)}$$

$$T_i \sim I^{0.33\pm0.04}{}_V 1.50\pm0.10_B{}^{-0.49\pm0.10} \quad \text{(HIP-1 } H^+\text{)}$$

$$T_i \sim I^{0.32\pm0.05}{}_B{}^{-0.30\pm0.12} \quad \text{(HIP-1 } D^+\text{)}$$

No scaling relation was obtained for helium in HIP-1 due to insufficient data. After the power law relation has been established, the statistical method used has the advantage that it is not necessary to hold two variables constant while varying a third when taking the data.

The second purpose of the study was to advance the theory of Doppler broadening of charge-exchange neutral spectra in rotating plasmas in mirror devices. It was shown that the order of making corrections is immaterial. Loss cones were found to increase the second moment. In the limit of zero ion-cyclotron radius, azimuthal drift decreased the second moment when the plasma was viewed across a diameter. This effect is opposite to and was obscured by the influence of finite cyclotron radius in the range of the ratio of drift to random energy reported previously. To obtain more accurate ion temperatures, drift will have to be included in the future.

The correction for a triangular slit function was found to be about the same as for a Gaussian slit function of the same width.

The use of the second moment instead of half width should facilitate obtaining the ion temperature where several kinds of charge-exchange processes produce a single charge-exchange line component.

APPENDIX A

LIST OF SYMBOLS

A	dummy variable
$B, \vec{B}$	midplane magnetic flux density
b_0, b_1, b_2, b_3, b_i	coefficients of net regression
c	velocity of light
D	integral in denominator of $\langle \Lambda^2 \rangle$ for loss cone and drift
D_1	first term in D
D_2	second term in D
E	total kinetic energy of ions
$\epsilon, \vec{\epsilon}$	electric field
F	line shape function
F_e	line shape function observed at exit slit
F_{e1}	F_e for $\lambda_m - \lambda_o < W$
F_{e2}	F_e for $\lambda_m - \lambda_o > W$
F_r	true line shape function
F_1	line shape function for fine structure at zero temperature
F_3	line shape function for fine structure component
g	$Wc(M/2kT)^{1/2}/\lambda_o$
H	$v_d(2M)^{1/2}/kT$
I	integrated intensity (spectral intensity integrated over all wavelengths)
k	Boltzmann's constant
M	mass of ion
N	integral in numerator of $\langle \Lambda^2 \rangle$ for loss cone and drift
N_1	first term in N
N_2	second term in N
n	number of charge-exchange processes
P	$v_d(M/2)^{1/2}$
Q	$HE^{1/2}$
R	mirror ratio

r	$\Lambda_m c(M/2kT)^{1/2}/\lambda_o$
S	slit function of monochromator
S_{T_i}	standard error of estimate of T_i
S_z	standard error of estimate of z
T_i	midplane ion temperature
U	$(R - 1)P/E^{1/2}R$
V	electrode voltage
v	velocity
v_c	cyclotron velocity
v_d	drift velocity
v_p	component of velocity parallel to $\vec{B}$
v_r	resultant velocity
v_x, v_y, v_z	components of v
W	full half width at half intensity of S in wavelength units
w	E/kT
x	difference between wavelength of light and monochromator setting, $\lambda - \lambda_m$
Y	$(R - 2(R - 1)P^2/E)^{1/2}/R$
y	distance from line of sight to centerline of test section (see fig. 4)
Z	$HE^{1/2}Y$
γ	$Mc^2\Lambda^2/2\lambda_o^2$
δ	Dirac delta function
ϵ	correction to second moment due to monochromator slit function
θ	polar angle in velocity space
θ_{c1}	θ for top of loss "cone" surface
θ_{c2}	θ for bottom of loss "cone" surface
$\Lambda, \Lambda', \Lambda'', \Lambda''', \Lambda''''$	displacement from center of charge-exchange component of spectral line, $\lambda - \lambda_o$
Λ_m	difference between wavelength set on monochromator and center of line, $\lambda_m - \lambda_o$
Λ_o	displacement of center of component from center of line
$\langle\Lambda^2\rangle_1$	apparent second moment of charge-exchange component of spectral line

$\langle \Lambda^2 \rangle_3$ $\langle \Lambda^2 \rangle_1$ corrected for monochromator slit function, magnetic splitting, and fine structure

λ wavelength of light

λ_m monochromator setting

λ_o wavelength of center of charge-exchange component of spectral line

σ_* charge-exchange cross section for excitation to electronically excited state

ϕ azimuthal angle in velocity space

ϕ_c ϕ for loss "cone" surface

Subscripts:

f fast

i fine structure component index

j process index

k number of fine structure components

n number of processes

t total

Special conventions:

$\langle\ \rangle$ average

APPENDIX B

DERIVATION OF SECOND MOMENT FOR DOPPLER-BROADENED CHARGE-EXCHANGE NEUTRAL SPECTRA AT THE MAGNETIC MIDPLANE WITH DRIFT AND LOSS CONES

When azimuthal drift is present in a magnetic mirror apparatus, the size of the loss cones is reduced (ref. 17) and they are no longer conical. Since the population of the loss cones is generally assumed to be negligible, and since the neutrals are assumed not to drift azimuthally, the second moment of charge-exchange spectra is not the same as for no drift and no loss cones even if the line of sight is across a diameter, as we will assume. We will also assume that the ion-cyclotron radius is zero (or, at least, is negligible).

From reference 17 the loss "cone" surfaces are defined at the magnetic midplane by

$$v_p^2 = v_c^2(R - 1) + v_d^2 \frac{R - 1}{R} \tag{B1}$$

where v_p is the component of ion and charge-exchange neutral velocity parallel to the magnetic field, v_c is the ion cyclotron velocity, and v_d is the ion azimuthal drift velocity (the charge-exchange neutral has the same velocities as the ion at the time of reaction but v_c becomes constant in direction). We adopt polar coordinates as shown in figure 14. Letting

$$P \equiv v_d \sqrt{\frac{M}{2}} \tag{B2}$$

and

$$E = \frac{1}{2} M v^2 \tag{B3}$$

equation (B1) can be solved for the value of ϕ on the loss "cone."

$$\phi_c = \sin^{-1}\left[\frac{1 - \dfrac{(R - 1)\left(\cos^2\theta - \dfrac{2P}{E^{1/2}} \cos\theta + \dfrac{R + 1}{R} \dfrac{P^2}{E}\right)}{1 - \cos^2\theta}}{R}\right]^{1/2} \tag{B4}$$

There are obviously limiting values of θ outside of which there are no loss cones. These are found by setting $\phi_c = 0$ in equation (B4) so

$$\cos \theta_{c1} = U + Y \tag{B5}$$

$$\cos \theta_{c2} = U - Y \tag{B6}$$

where

$$U \equiv \frac{(R - 1)P}{E^{1/2}R} \tag{B7}$$

and

$$Y \equiv \frac{\left[R - 2(R - 1)\frac{P^2}{E}\right]^{1/2}}{R} \tag{B8}$$

There is a limiting value of E (or v) below which there are no loss "cones." This is found by setting $\theta_{c1} = \theta_{c2}$ in equations (B5) and (B6) with the result

$$E_c = \frac{2(R - 1)P^2}{R} \tag{B9}$$

The second moment is given by

$$\left\langle \Lambda^2 \right\rangle = \frac{\lambda_o^2}{c^2} \left\langle v_x^2 \right\rangle \tag{B10}$$

where the average is over the charge-exchange neutral velocity distribution function, the unnormalized version of which is assumed to be (in Cartesian coordinates and for plasma along the line of sight and to the right of the vertical centerplane (fig. 4))

$$\sigma_* (v) v e^{-\left[M/2kT\right]\left[v_x^2 + (v_y - v_d)^2 + v_z^2\right]} \tag{B11}$$

which is a Maxwell-Boltzmann distribution with a drift correction and a $\sigma_* v$ correction. From equations (B10) and (B11)

$$\langle \Lambda^2 \rangle = \frac{2\lambda_o^2}{Mc^2} \frac{\int E^2 \sigma_* e^{-E/kT} \int \sin^3\theta e^{HE^{1/2}\cos\theta} \int \sin^2\phi \, d\phi \, d\theta \, dE}{\int E\sigma_* e^{-E/kT} \int \sin\theta e^{HE^{1/2}\cos\theta} \int d\phi \, d\theta \, dE} \tag{B12}$$

where

$$H \equiv \frac{v_d (2M)^{1/2}}{kT} \tag{B13}$$

If we call the triple integrals in the numerator and denominator of equation (B12) N and D, respectively, then

$$\langle \Lambda^2 \rangle = \frac{2\lambda_o^2}{Mc^2} \frac{N}{D} \tag{B14}$$

By symmetry it is only necessary to integrate N and D over the range

$$0 \leq \theta \leq \pi$$

$$0 \leq \phi \leq \frac{\pi}{2}$$

$$0 \leq E \leq \infty$$

excluding the loss cones. This gives

$$N = \frac{\pi N_1}{2H^2} + \frac{N_2}{4} \tag{B15}$$

where

$$N_1 = 2 \int_0^{E_c} E\sigma_* e^{-E/kT} \left(\cosh Q - \frac{\sinh Q}{Q} \right) dE \tag{B16}$$

$$N_2 = \int_{E_c}^{\infty} E^2\sigma_* \left[\frac{\pi}{Q} e^{-E/kT} \left\{e^{QU}\left[2(U^2 + Y^2 - 1) \sinh Z \right.\right.\right.$$

$$\left.\left.\left. + 4Y \left(U - \frac{1}{Q}\right) \left(\cosh Z - \frac{\sinh Z}{Z}\right)\right] + \frac{4}{Q} \left(\cosh Q - \frac{\sinh Q}{Q}\right)\right\}\right.$$

$$+ e^{-E/kT} \int_{\cos\theta_{c2}}^{\cos\theta_{c1}} (1 - \cos^2\theta) e^{Q\cos\theta} [\pi - 2\phi_c$$

$$\left. + \sin (2\phi_c)] \, d (\cos \theta)\right] dE \qquad \text{(B17)}$$

where

$$Q \equiv HE^{1/2} \qquad \text{(B18)}$$

$$Z \equiv HE^{1/2}Y \qquad \text{(B19)}$$

Similarly

$$D = \frac{\pi}{2} (D_1 + D_2) \qquad \text{(B20)}$$

where

$$D_1 = \int_0^{E_c} \frac{2E\sigma_*}{Q} e^{-E/kT} \sinh Q \, dE \qquad \text{(B21)}$$

$$D_2 = \int_{E_c}^{\infty} E\sigma_* \left[\frac{2}{Q} e^{-E/kT}(\sinh Q - e^{QU} \sinh Z)\right.$$

$$\left. + e^{-E/kT} \int_{\cos\theta_{c2}}^{\cos\theta_{c1}} e^{Q\cos\theta} \left(1 - \frac{2\phi_c}{\pi}\right) d (\cos \theta)\right] dE \qquad \text{(B22)}$$

Hence $\langle \Delta^2 \rangle$ is calculated from equations (B2), (B4) to (B9), and (B13) to (B22). For small arguments, expressions of the form cosh A - sinh A/A should be expanded in power series to avoid loss of accuracy.

The above derivation is for the plasma to the right of the vertical center plane. However, along a diameter the plasma to the left of the vertical center plane produces the same symmetrical unshifted line shape and second moment as the plasma to the right.

APPENDIX C

DERIVATION OF SECOND MOMENT CORRECTION DUE TO TRIANGULAR SLIT FUNCTION OF MONOCHROMATOR

The apparent second moment should be corrected for the slit function of the monochromator. We assume a triangular slit function S (fig. 12) for a monochromator set at λ_m. The slit function is symmetric about λ_m and is given by

$$S = \frac{\lambda - \lambda_m + W}{W^2} \qquad (\lambda_m - W \leq \lambda \leq \lambda_m) \tag{C1}$$

$$S = \frac{\lambda_m - \lambda + W}{W^2} \qquad (\lambda_m + W \geq \lambda \geq \lambda_m) \tag{C2}$$

We assume the line shape F before passing through the monochromator is the shape for a constant charge-exchange cross section (since the order of convolutions does not matter, as proved in the section IMPROVED THEORY OF LINE SHAPES AND SECOND MOMENTS, fine structure and/or magnetic splitting can be hypothetically removed before passing through the monochromator). From equation (B7) of reference 2 this is

$$F(\lambda - \lambda_o) = \frac{M^{1/2} c}{\lambda_o (2kT)^{1/2}} \int_{(\gamma/kT)^{1/2}}^{\infty} w^2 e^{-w^2} \, dw \tag{C3}$$

where $w^2 = E/kT$. From equation (D6) of reference 2 the apparent line shape is

$$F_e(\lambda_m - \lambda_o) = \int_0^{\infty} F(\lambda - \lambda_o) S(\lambda_m - \lambda) \, d\lambda \tag{C4}$$

Substituting equations (C1) to (C3) into (C4) gives

$$F_e(\lambda_m - \lambda_o) = \frac{M^{1/2} c}{W^2 \lambda_o (2kT)^{1/2}} \left[\int_{\lambda_m - W}^{\lambda_m} \int_{(\gamma/kT)^{1/2}}^{\infty} w^2 e^{-w^2} \, dw (\lambda - \lambda_m + W) \, d\lambda \right.$$

$$\left. + \int_{\lambda_m}^{\lambda_m + W} \int_{(\gamma/kT)^{1/2}}^{\infty} w^2 e^{-w^2} \, dw (\lambda_m - \lambda + W) \, d\lambda \right] \tag{C5}$$

This will be evaluated only for the case $\lambda_m \geq \lambda_o$ because the case $\lambda_m \leq \lambda_o$ will be symmetric. For $\lambda_m \geq \lambda_o$ there are two subcases as shown in figure 19. For cases (a) and (b) we designate the apparent line shapes by F_{e1} and F_{e2}, respectively.

$$F_{e1}(\lambda_m - \lambda_o) = \frac{M^{1/2}c}{W^2\lambda_o(2kT)^{1/2}}\left[\int_{\lambda_m-W}^{\lambda_o}\int_{-(\gamma/kT)^{1/2}}^{\infty} w^2e^{-w^2}\,dw(\lambda - \lambda_m + W)\,d\lambda\right.$$

$$+\int_{\lambda_o}^{\lambda_m}\int_{(\gamma/kT)^{1/2}}^{\infty} w^2e^{-w^2}\,dw(\lambda - \lambda_m + W)\,d\lambda$$

$$\left.+\int_{\lambda_m}^{\lambda_m+W}\int_{(\gamma/kT)^{1/2}}^{\infty} w^2e^{-w^2}\,dw(\lambda_m - \lambda + W)\,d\lambda\right] \qquad (C6)$$

$$F_{e2}(\lambda_m - \lambda_o) = \frac{M^{1/2}c}{W^2\lambda_o(2kT)^{1/2}}\left[\int_{\lambda_m-W}^{\lambda_m}\int_{(\gamma/kT)^{1/2}}^{\infty} w^2e^{-w^2}\,dw(\lambda - \lambda_m + W)\,d\lambda\right.$$

$$\left.+\int_{\lambda_m}^{\lambda_m+W}\int_{(\gamma/kT)^{1/2}}^{\infty} w^2e^{-w^2}\,dw(\lambda_m - \lambda + W)\,d\lambda\right] \qquad (C7)$$

Letting $\Lambda_m = \lambda_m - \lambda_o$, the second moment of F_e is

$$\left\langle \Lambda_m^2 \right\rangle = 2\left[\int_0^W \Lambda_m^2 F_{e1}(\Lambda_m)\,d\Lambda_m + \int_W^{\infty} \Lambda_m^2 F_{e2}(\Lambda_m)\,d\Lambda_m\right] \qquad (C8)$$

Let

$$r \equiv \frac{\Lambda_m c}{\lambda_o}\left(\frac{M}{2kT}\right)^{1/2} \qquad (C9)$$

and

$$g \equiv \frac{Wc}{\lambda_o}\left(\frac{M}{2kT}\right)^{1/2} \tag{C10}$$

So equation (C8) becomes

$$\left\langle \Lambda_m^2 \right\rangle = 2\left(\frac{2\lambda_o^2 kT}{Mc^2}\right)^{3/2}\left[\int_0^g r^2 F_{e1}(r)\,dr + \int_g^\infty r^2 F_{e2}(r)\,dr\right] \tag{C11}$$

This can be integrated with difficulty to give

$$\left\langle \Lambda_m^2 \right\rangle = \frac{2}{3}\left(\frac{2\lambda_o^2 kT}{Mc^2}\right)\left(1 + \frac{g^2}{4}\right) \tag{C12}$$

But this is simply

$$\left\langle \Lambda_m^2 \right\rangle = \left\langle \Lambda^2 \right\rangle_3 + \frac{W^2}{6} \tag{C13}$$

where $\left\langle \Lambda^2 \right\rangle_3$ is the second moment of F. We assume equation (C13) is a good approximation even if σ_* is not exactly constant.

APPENDIX D

DERIVATION OF SECOND MOMENT FOR DOPPLER-BROADENED CHARGE-EXCHANGE NEUTRAL SPECTRA WITH SEVERAL SUPERIMPOSED PROCESSES

We assume that the line shapes F_j of several charge-exchange processes $j = 1,2,\ldots,n$ are superimposed. We do not assume that the F_j have the same shape, same second moments, or same centers. It is desired to find the second moment $\langle \lambda^2 \rangle_t$ of the line shape resulting from superposition.

The intensity of component j resulting from process j at wavelength λ is proportional to $I_j F_j$, where I_j is the integrated intensity of component j normalized by

$$\sum_{j=1}^{n} I_j = 1 \tag{D1}$$

The wavelength λ_o of the center of the line shape for the superposition is

$$\lambda_o = \frac{\int_0^\infty \lambda \sum_{j=1}^{n} I_j F_j \, d\lambda}{\int_0^\infty \sum_{j=1}^{n} I_j F_j \, d\lambda} \tag{D2}$$

We define the center of profile j by

$$\lambda_{oj} \equiv \int_0^\infty \lambda F_j \, d\lambda \tag{D3}$$

so equation (D2) becomes

$$\lambda_o = \sum_{j=1}^{n} I_j \lambda_{oj} \tag{D4}$$

Obviously

$$\langle \Lambda^2 \rangle_t = \frac{\int_0^\infty (\lambda - \lambda_o)^2 \sum_{j=1}^{n} I_j F_j \, d\lambda}{\int_0^\infty \sum_{j=1}^{n} I_j F_j \, d\lambda} \tag{D5}$$

If we define the second moment of component j by

$$\langle \Lambda^2 \rangle_j = \int_0^\infty (\lambda - \lambda_{oj})^2 F_j \, d\lambda \tag{D6}$$

and define

$$\Lambda_{oj} \equiv \lambda_{oj} - \lambda_o \tag{D7}$$

then equation (D5) becomes

$$\langle \Lambda^2 \rangle_t = \sum_{j=1}^{n} I_j \left(\langle \Lambda^2 \rangle_j + \Lambda_{oj}^2 \right) \tag{D8}$$

REFERENCES

1. A. Hirose and I. Alexeff, Nuc. Fusion 12 (1972) 315.

2. R. W. Patch, et al., NASA TM X-71635 and Bull. Am. Phys. Soc. 19 (1974) 975.

3. W. R. Hess, Phys. Lett. 34A (1971) 367.

4. D. R. Sigman and J. J. Reinmann, NASA TM X-2783 (1973).

5. J. J. Reinmann et al., IEEE Trans. Plasma Sci. PS-3 (1975) 6.

6. I. Alexeff et al., Phys. Rev. Ltrs. 23 (1969) 281.

7. G. W. Englert, J. J. Reinmann, and M. R. Lauver, Plasma Physics (1975) 609.

8. G. W. Englert, R. W. Patch, and J. J. Reinmann, Bull. Am. Phys. Soc. 20 (1975) 1322.

9. J. J. Reinmann, et al., NASA TM X-71852 (1975).

10. J. J. Reinmann, et al., Fifth Symp. on Engineering Problems of Fusion Research (Inst. Electronics and Electrical Engrs., New York, 1974) 587.

11. F. C. Mills, Statistical Methods Applied to Economics and Business (Holt, New York, 1924) 485.

12. S. M. Sidik, NASA TN D-6770 (1972).

13. W. J. Dixon and F. J. Massey, Introduction to Statistical Analysis (McGraw-Hill, New York, 1957).

14. E. W. Thomas, Excitation in Heavy Particle Collisions (Wiley-Interscience, New York, 1972) 7 and 60.

15. H. R. Griem, Plasma Spectroscopy (McGraw-Hill, New York, 1964) 101.

16. R. Lincke, Plasma Diagnostics, W. Lochte-Holtgreven, ed. (North-Holland, Amsterdam, 1968) 347.

17. K. Boyer, et al., Proc. 2nd United Nations Intern. Conf. on the Peaceful Uses of Atomic Energy (United Nations, Geneva, 1958) 319.

TABLE I. - RANGE OF TEST CONDITIONS AND ION TEMPERATURES

Apparatus	Gas	Midplane magnetic flux density, B, tesla	Electrode voltage, V, KV	Total current, I, A	Pressure of neutrals, torr	Midplane ion temperature, T_i, eV
SUMMA	H_2	2.07 to 2.49	7.1 to 19.6	0.60 to 1.10	8.8×10^{-5} to 1.1×10^{-4}	169 to 854
	He	2.07 to 2.46	4.9 to 19.9	0.82 to 1.06	1.3×10^{-4} to 2.0×10^{-4}	666 to 4927
HIP-1	H_2	0.75 to 1.12	12.0 to 22.4	0.49 to 1.92	5.4×10^{-5} to 1.3×10^{-4}	170 to 607
	D_2	0.60 to 1.14	22.0	0.21 to 1.08	6.9×10^{-5} to 1.0×10^{-4}	268 to 650
	He	0.81 to 1.10	17.0 to 22.0	0.38 to 1.28	1.4×10^{-4} to 1.7×10^{-4}	597 to 980

TABLE II. - STATISTICAL SUMMARY OF SCALING RELATIONS

Apparatus	Gas	Sample size	Independent variable	Sample partial correlation coefficient	Level of significance	Correlation significant?	Standard deviation of coefficient of net regression	Standard error of estimate of log T_i, S_z
SUMMA	H_2	24	Overall					0.0298
			I	0.760	<0.001	Highly significant	0.10	
			V	0.989	<0.001	Highly significant	0.05	
			B	-0.801	<0.001	Highly significant	0.22	
SUMMA	He	38	Overall					0.0453
			I	-0.076	0.663	Not significant	0.24	
			V	0.976	<0.001	Highly significant	0.05	
			B	-0.216	0.205	Not significant	0.22	
HIP-1	H_2	88	Overall					0.0485
			I	0.687	<0.001	Highly significant	0.04	
			V	0.855	<0.001	Highly significant	0.10	
			B	-0.472	<0.001	Highly significant	0.10	
HIP-1	D_2	42	Overall					0.0593
			I	Not available	<0.001	Highly significant	0.05	
			B		0.016	Significant	0.12	

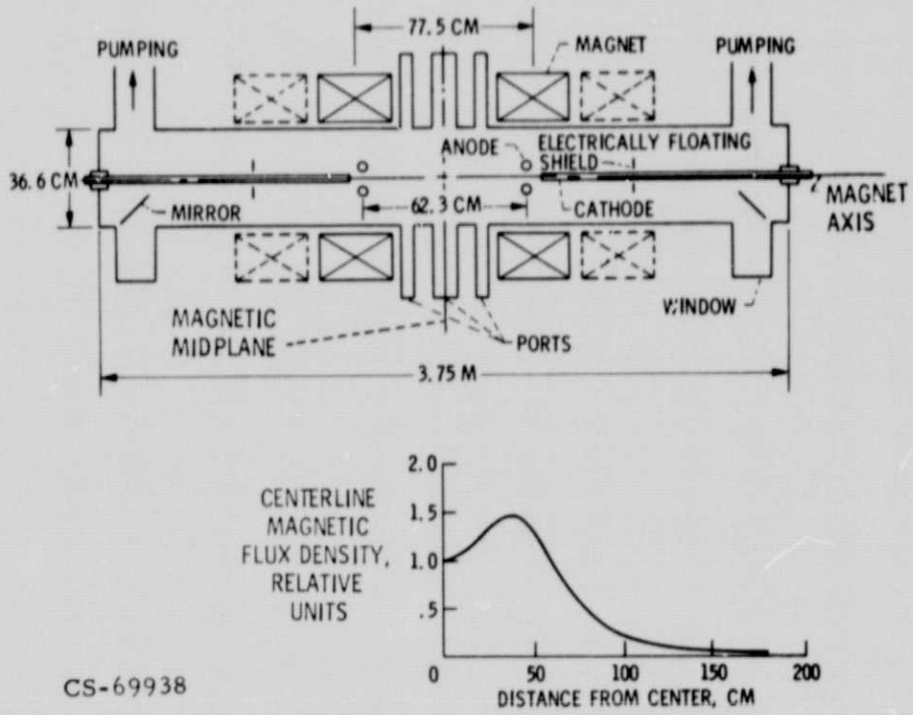

Figure 1. - Test section and magnetic field configuration for SUMMA.

E-8604

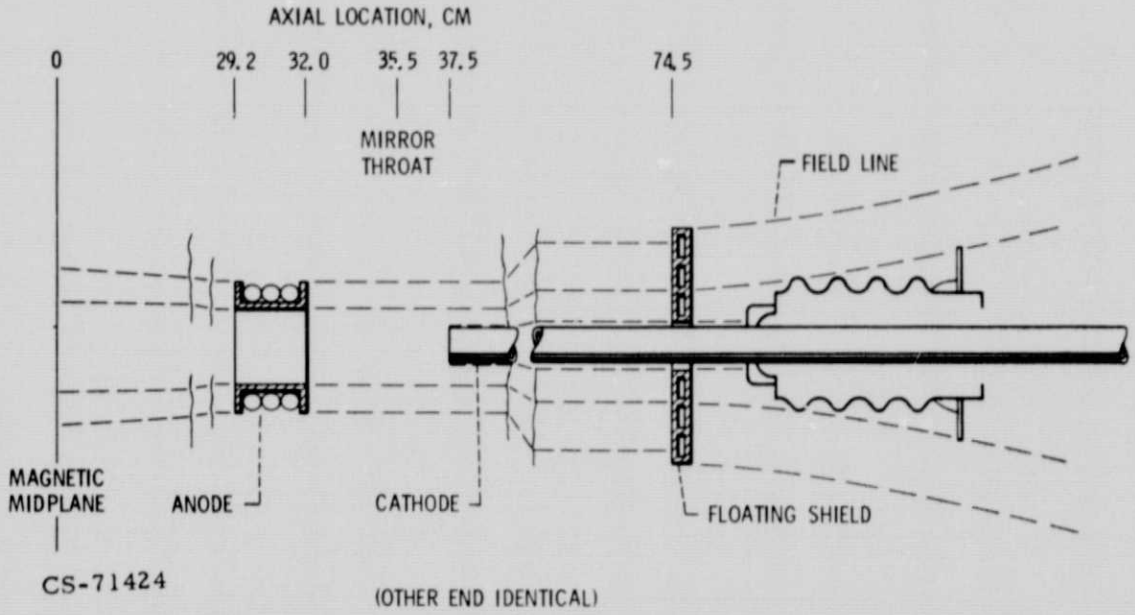

Figure 2. - Electrode configuration and magnetic field lines for SUMMA.

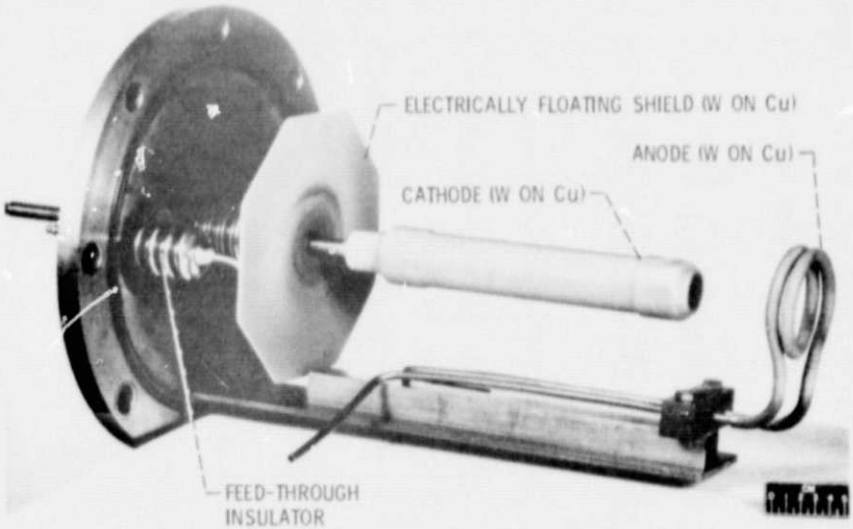

Figure 3. - HIP-1 electrode assembly (one of two).

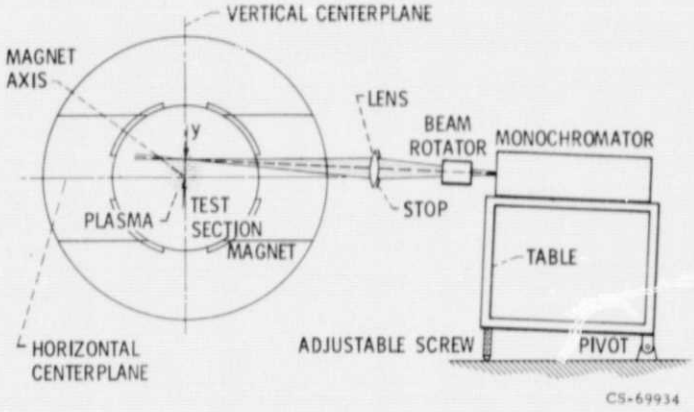

Figure 4. - Apparatus for Doppler broadening measurements. (Not to scale.)

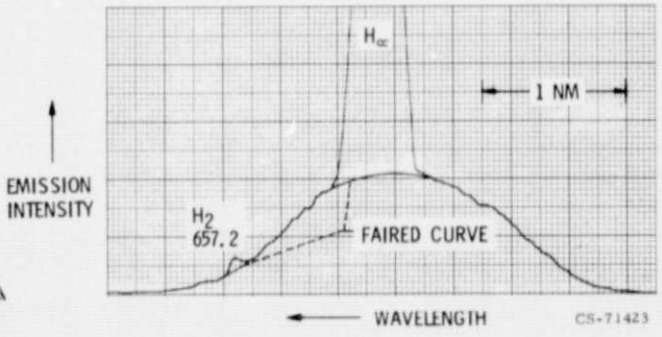

Figure 5. - Typical H_α line exhibiting wide and narrow components.

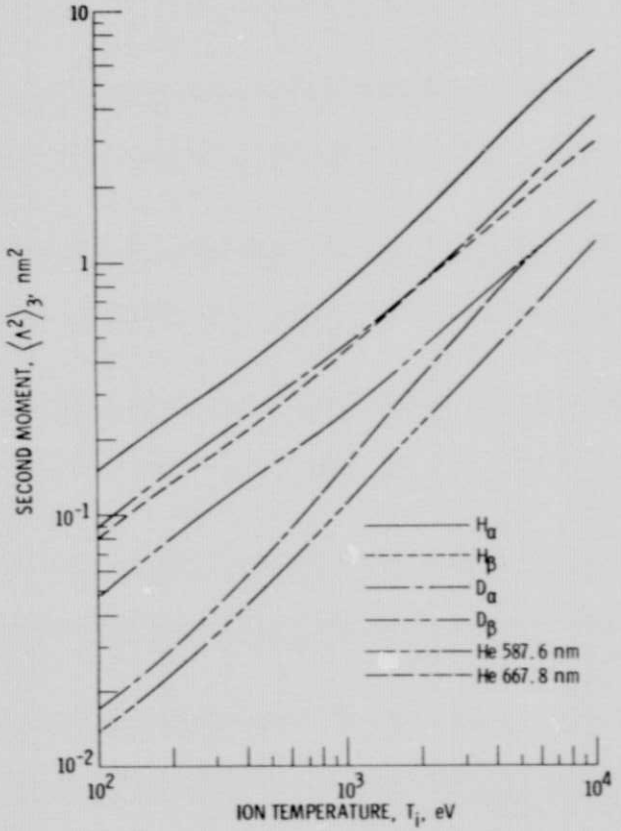

Figure 6. - Calculated second moments of wide components of six lines in limit of zero ion-cyclotron radius. $V_d = 0$; $R = \infty$.

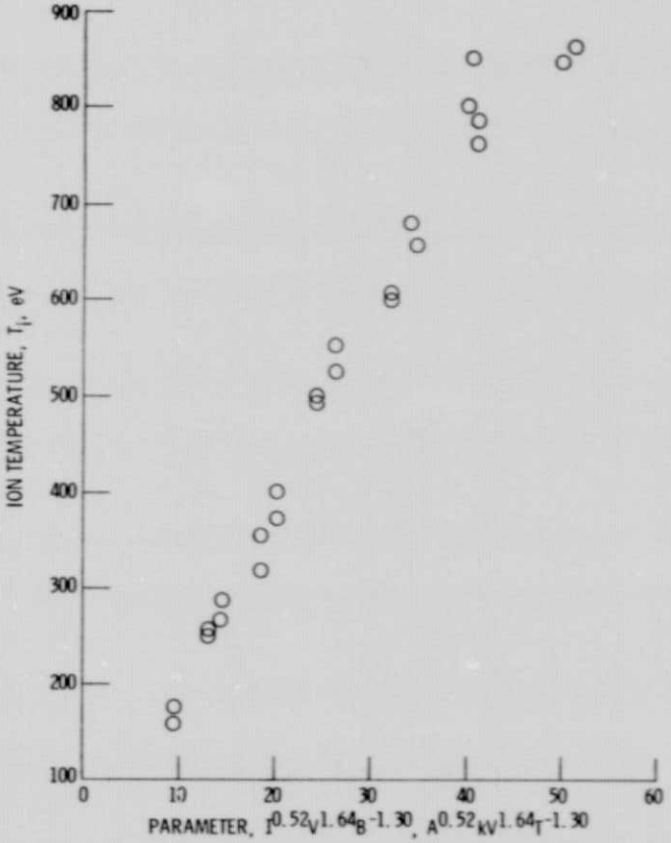

Figure 7. - H^+ ion temperature scaling relation for SUMMA.

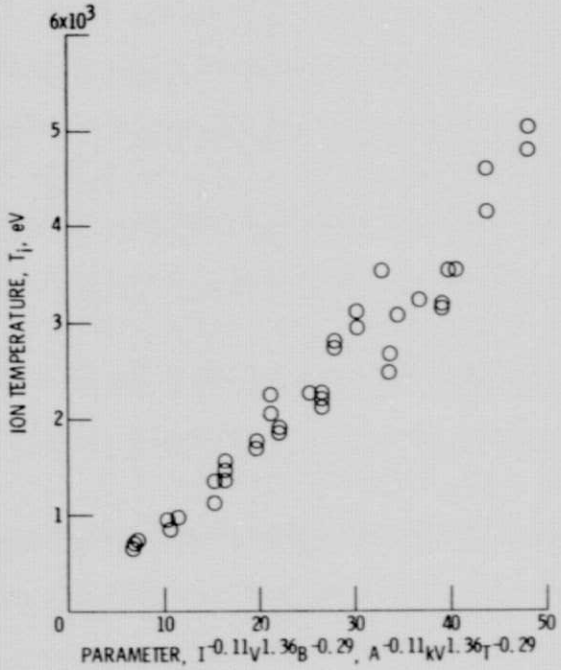

Figure 8. - He^+ ion temperature scaling relation for SUMMA.

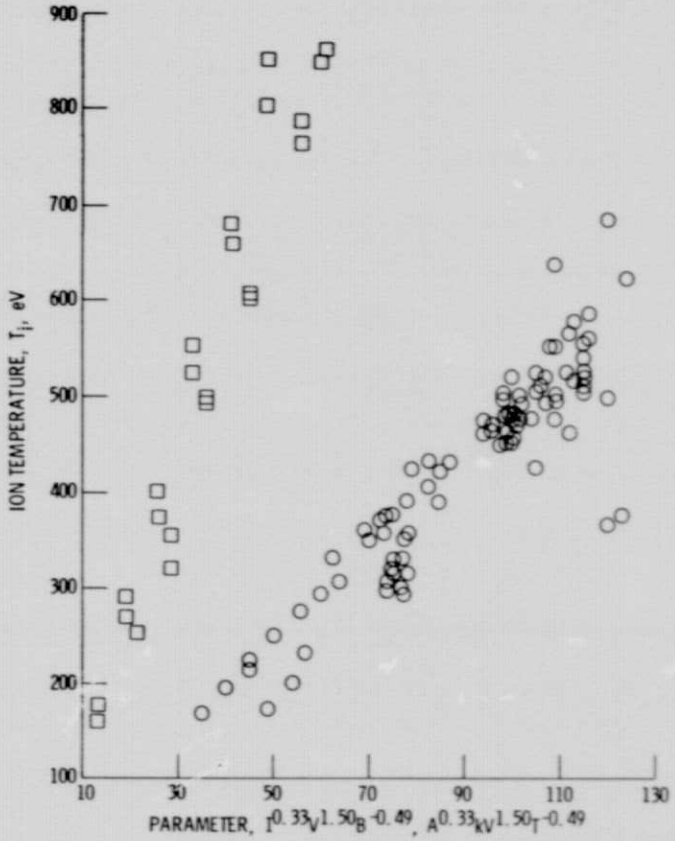

Figure 9. - H^+ ion temperature scaling relation for HIP-1 and comparison with SUMMA.

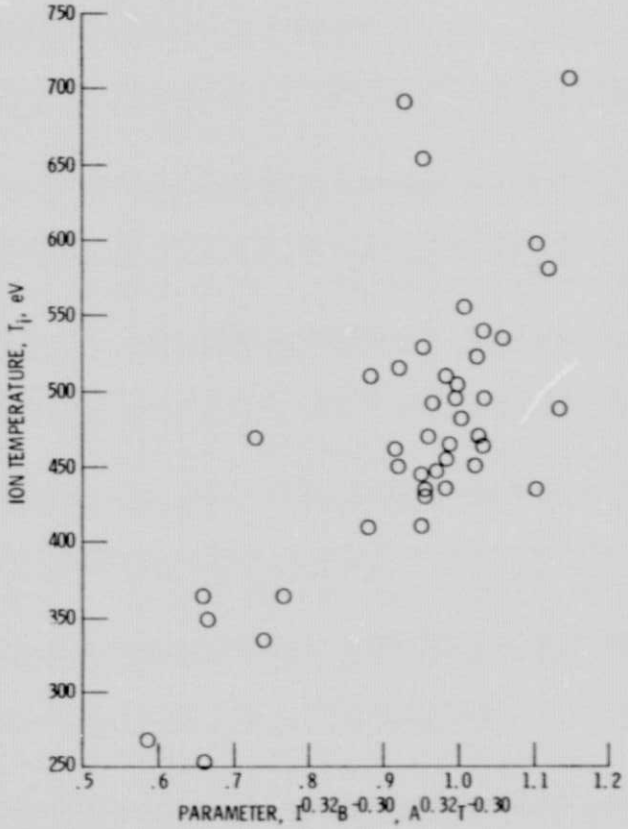

Figure 10. - D^+ ion temperature scaling relation for HIP-1. V = 22 kV.

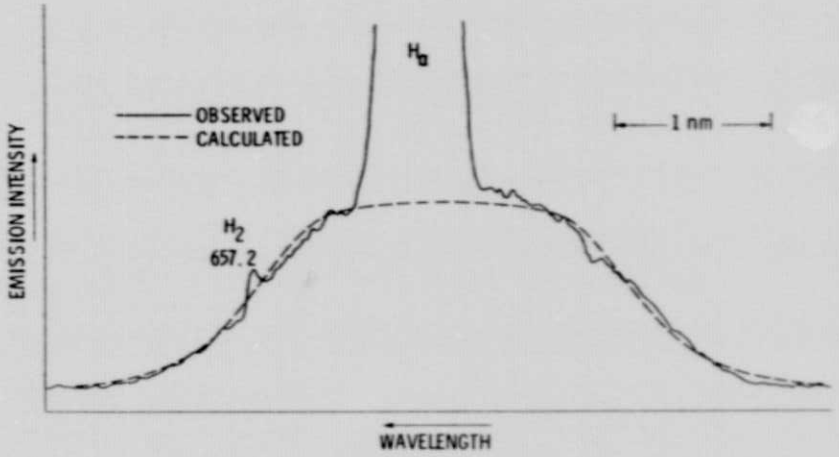

Figure 11. - Comparison of observed and calculated wide component of H_α. I = 1.1 A, V = 19.2 kV, B = 2.49 T.

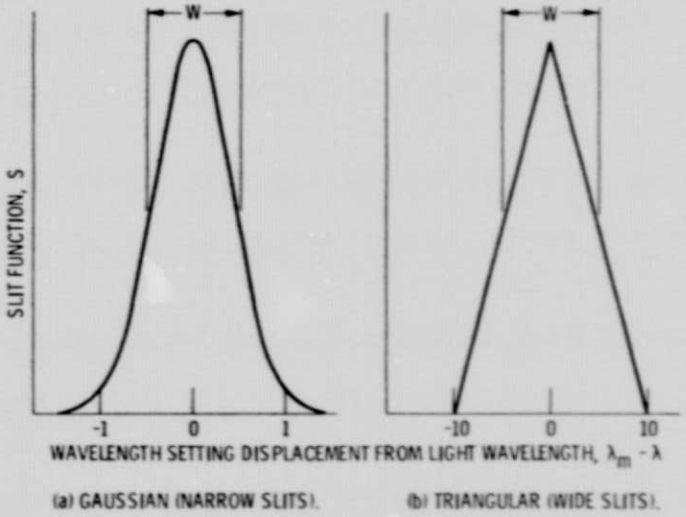

Figure 12. - Typical monochromator slit functions for two slit widths. (Entrance slit width = exit slit width; not to scale.)

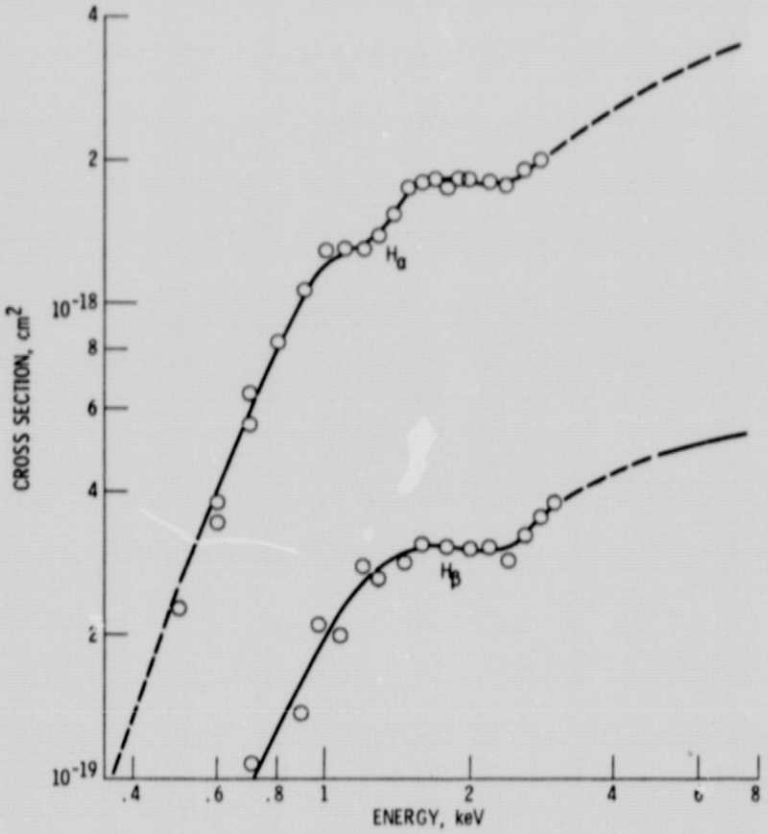

Figure 13. - Charge-exchange cross sections (ref. 2). $H^+ + H_2 \rightarrow H^0 + H_2^+$.

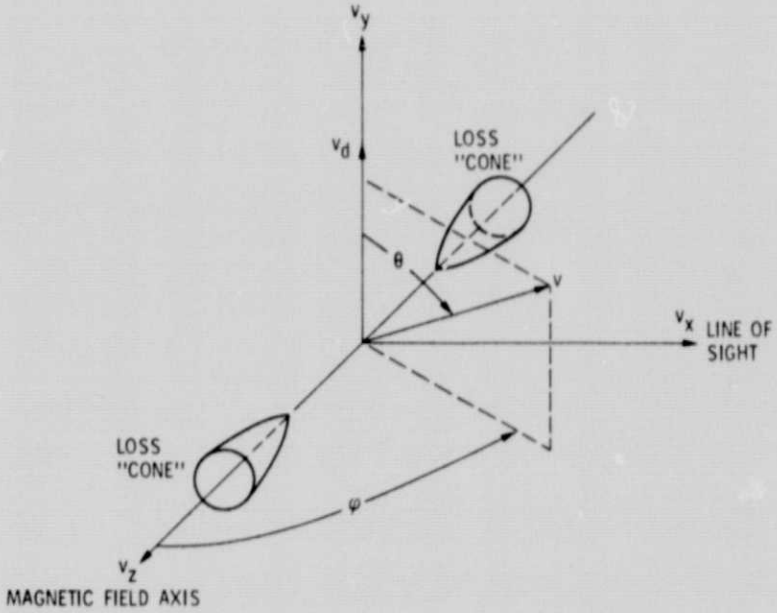

Figure 14. - Cartesian and polar coordinates in velocity space for derivation of second moment with drift and loss "cones."

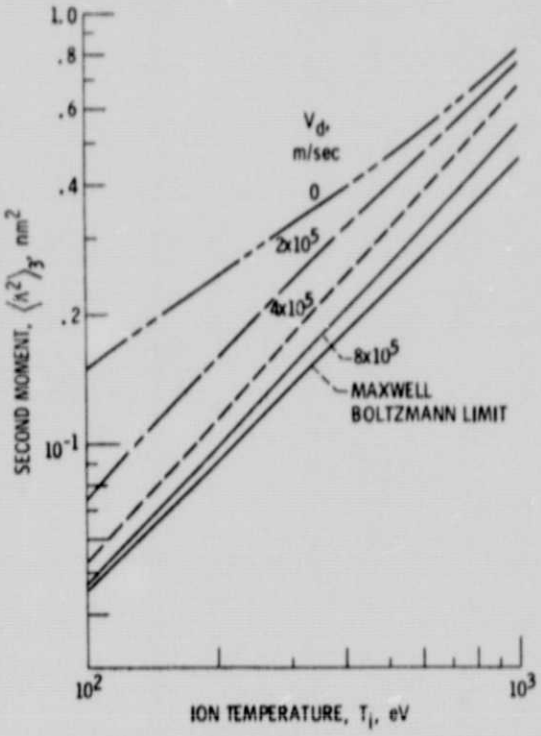

Figure 15. - Effect of drift on second moment of H_a in limit of zero ion-cyclotron radius. $R = \infty$.

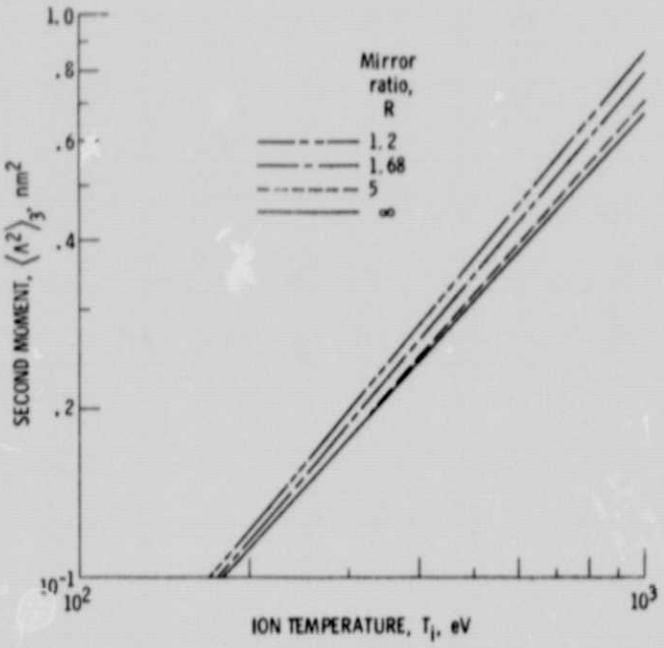

Figure 16. - Effect of mirror ratio on second moment of H_a at magnetic midplane in limit of zero ion-cyclotron radius. V_d = 400 000 m/sec.

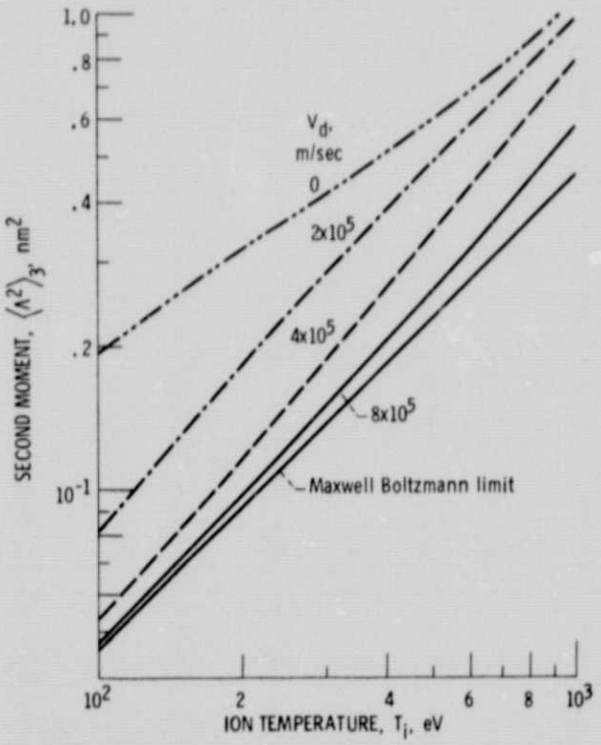

Figure 17. - Effect of drift on second moment of H_a at the magnetic midplane in the limit of zero ion-cyclotron radius. $R = 1.68$.

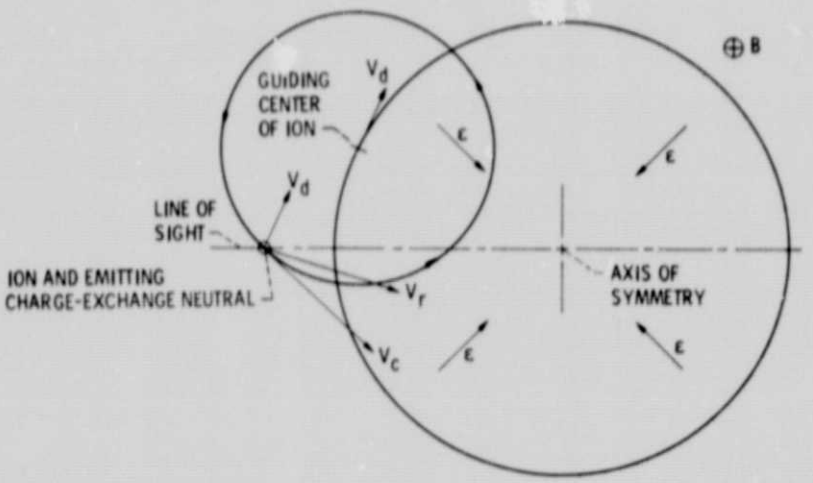

Figure 18. - Cause of line broadening due to finite ion-cyclotron radius combined with azimuthal drift. (Not to scale.)

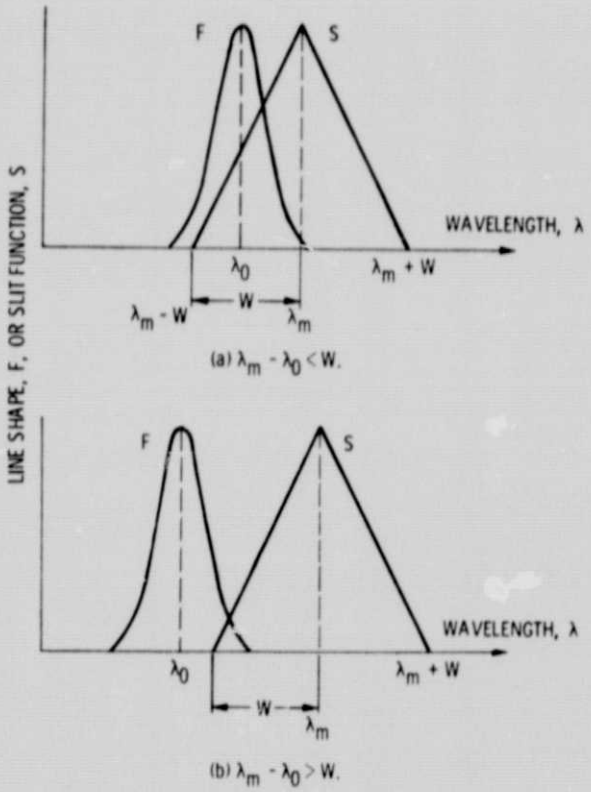

Figure 19. - Two subcases in the calculation of the second moment correction due to triangular slit function. (Not to scale.)